

See discussions, stats, and author profiles for this publication at: <https://www.researchgate.net/publication/284013903>

A computational model for a rocket mass heater

Article in *Applied Thermal Engineering* · October 2015

DOI: 10.1016/j.applthermaleng.2015.10.035

CITATIONS

0

READS

883

1 author:



[Mark R Schumack](#)

University of Detroit Mercy

24 PUBLICATIONS 161 CITATIONS

SEE PROFILE

All content following this page was uploaded by [Mark R Schumack](#) on 15 February 2016.

The user has requested enhancement of the downloaded file. All in-text references [underlined in blue](#) are added to the original document and are linked to publications on ResearchGate, letting you access and read them immediately.



Research Paper

A computational model for a rocket mass heater

Mark Schumack*

Mechanical Engineering Department, University of Detroit Mercy, 4001 W. McNichols, Detroit, MI 48221, USA



HIGHLIGHTS

- A simple one dimensional transient model of a rocket mass heater is presented.
- Heat transfer and fluid friction through important geometric features are considered.
- Introducing a system damper and increasing duct length can improve efficiency.
- Low chimney height and small barrel clearances can threaten heater performance.

ARTICLE INFO

Article history:

Received 20 July 2015

Accepted 10 October 2015

Available online 19 October 2015

Keywords:

Rocket mass heater

Masonry heater

Rocket stove

Biomass stove

Thermal modeling

ABSTRACT

A simple one dimensional pseudo-steady computational model of a rocket mass heater is presented. A rocket mass heater is a space heating device that utilizes an insulated “J-tube” to promote complete combustion of burning wood, a steel barrel to act as a heat radiator, and a thermal mass usually shaped into a bench that stores heat from the exhaust before the combustion gases are released to the atmosphere. The gas model is based on fundamental relationships for steady compressible flow through one-dimensional geometry and is coupled to an unsteady finite difference model for two dimensional heat conduction in the thermal mass, which is modeled as a hollow cylinder. The model accounts for detailed heat transfer effects and fluid frictional losses, and is able to predict efficiency, flow rate, and spatial variations in temperature and pressure as functions of key parameters such as burn rate, thermal mass volume and length, duct routing details, and chimney height. Key results demonstrate how insufficient chimney height and narrow barrel clearances can threaten heater performance, how a system damper and increasing duct length can improve heater efficiency, and that axial temperature variation in the mass is small compared to radial gradients.

© 2015 Published by Elsevier Ltd.

1. Introduction

Over the last decade, rocket mass heaters (RMHs) have gained popularity as space heating alternatives for those interested in sustainable home design, natural building, or off-grid living. These custom built units consist of an insulated burn chamber, tunnel, and heat riser (together called the “J-tube”) covered by a steel barrel, followed by a long exhaust duct – sometimes up to 10 m long – embedded in a thermal mass leading to a chimney which exhausts the combustion gases to the outdoors. The adiabatic J-tube is designed to ensure high temperatures to promote complete combustion of the wood fuel. The steel barrel is typically a 0.2 m³ drum which serves as a radiation heat source for the space, and whose top can also serve as a cooking surface. The thermal mass which encloses the exhaust duct and absorbs heat from the hot combustion gases is normally made of “cob,” which is a clay and sand mixture

reinforced with straw. The thermal mass is often sculpted into a bench which becomes an integral architectural feature of the home, radiating thermal energy into the space long after the fire has gone out. A photograph of a typical RMH is shown in Fig. 1. Fig. 2 illustrates the RMH schematically and shows the flow path of the gases through the heater.

RMH designs are based on features of the “rocket stove” and masonry heater. A rocket stove is a cooking appliance optimized to provide relatively high heat utilization and low emissions. A large amount of research has gone into improving cookstove performance in order to mitigate resource and health challenges in developing countries [1,2]. Significant features of such stoves include a horizontal burn chamber and insulated short chimney located under the cooking pot. Masonry heaters have been used since pre-historic times and have evolved into various designs in Europe, Russia, and China [3]. The key principle is the incorporation of a large thermal mass built of masonry which absorbs heat from exhausting combustion products directed in a sinuous path through channels embedded in the masonry. After an initial heat-up period, a masonry heater releases thermal energy to the space by radiation for over 24 hours after the wood fuel is exhausted.

* Corresponding author. Tel.: +(313) 993-3370; fax: +(313) 993-1187.
E-mail address: schumamr@udmercy.edu.



Fig. 1. Rocket mass heater in Michigan. The burn chamber inlet is the black opening in front of the barrel. Approximately 4 m of horizontal duct is embedded in the cob bench. The horizontal duct leaves the manifold at the bottom of the barrel behind the pillar on the left, wraps around the pillar, runs left to right within the front part of the bench, makes a 90° turn through the cleanout on the right, then runs back along the wall on the right before making a turn to the left to enter the vertical chimney just to the right of the barrel.

Bryden et al. [4] described design principles for wood burning cookstoves. The authors presented ten design principles, including the need for an insulated burn chamber and short chimney underneath the cooking surface, the importance of maintaining a strong draft to ensure high temperatures and clean emissions, and the necessity for all flow passages in the stove to have the same cross-sectional area. The “double barrel rocket stove” described in Bryden et al. [5] introduced the downdraft principle in which hot gases rising through an insulated chimney are directed downward through the annular space between two steel barrels, providing a large surface for radiant heat transfer to the space. Evans and Jackson [6] are the first to have published design guidelines for RMHs which combined the downdraft principle with long runs of exhaust ducting embedded in cob. Over the last decade, many resources have appeared for do-it-yourselfers interested in design and construction, including workshops [7] and online forums [8].

Despite the interest in RMHs, little has been published regarding performance measurements or analytical modeling. Menghini et al. [9] performed a CFD analysis on a fireplace wood heater and used the CFD results to develop a simplified zone model with physical relationships for combustion and conductive, convective, and radiation heat transfer at various locations within the unit. Felaco and Gasser [10] presented an unsteady one-dimensional model for gas dynamics in a chimney. They applied an explicit upwind finite difference method to a straight vertical chimney, and accounted for fluid friction and nonadiabatic chimney walls using a reduced form

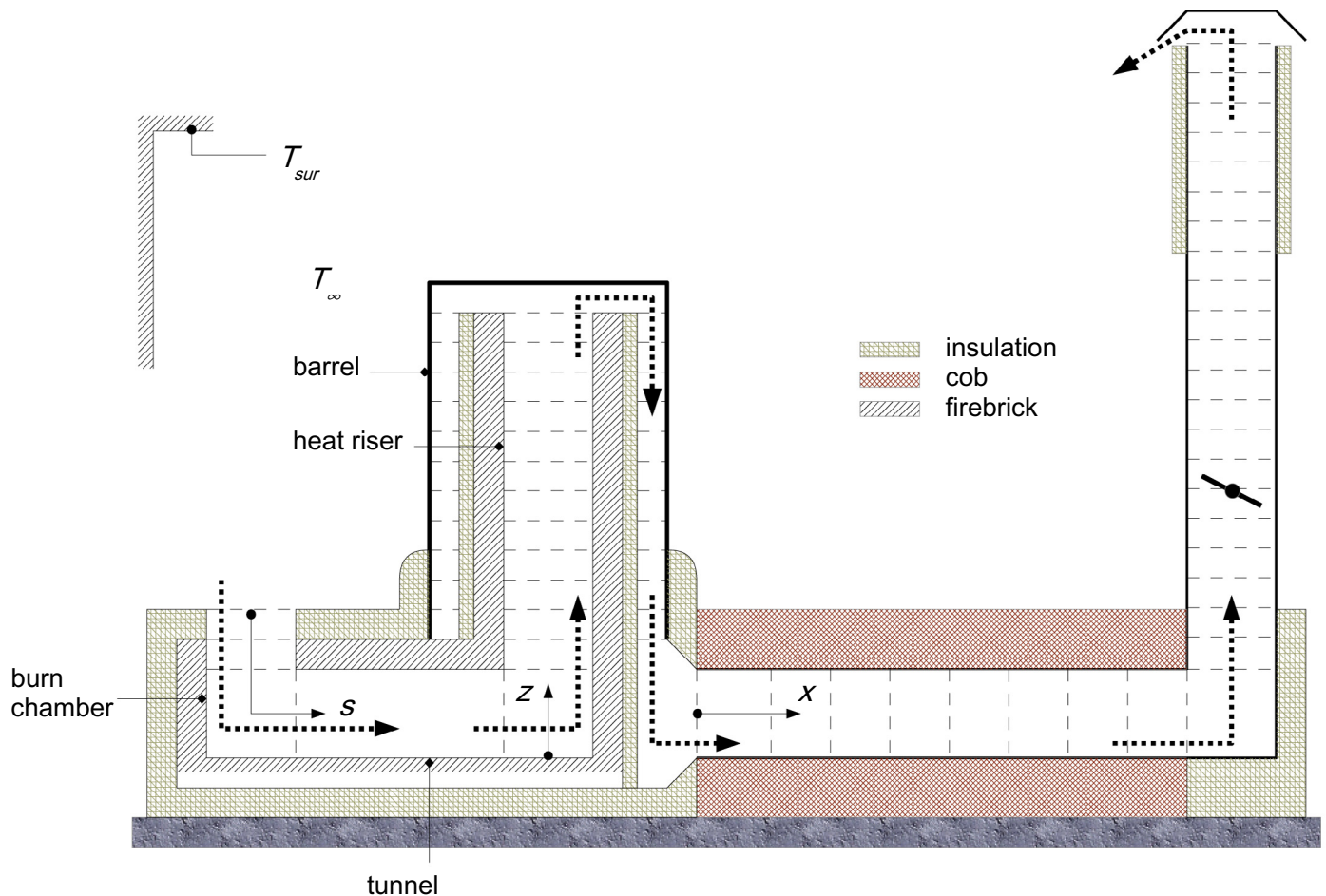


Fig. 2. Schematic of the simplified RMH geometry. The dashed lines indicate possible placements for elemental nodes, and dotted lines with arrowheads indicate flow direction. Note that fittings, like the elbows in the J-tube and the transition from annulus to horizontal duct, are not discretized but instead modeled with adiabatic loss coefficients. Logs are placed vertically in the burn chamber on the left, and combustion is modeled as a heat source in bottom of the burn chamber.

of the compressible flow equations for low Mach number flows. Saastamoinen et al. [11] presented a simplified model for the heat released during combustion in a residential wood burning stove. This calculated value was then used as an input to an analytical treatment of the stove walls in order to determine the heat output to the heated space. MacCarty and Bryden [12] reviewed models for cookstoves. MacCarty [13] and MacCarty and Bryden [14] described a zonal model for a cookstove, using correlations for various losses including fluid friction, and presented convective heat transfer relations for various parts of the geometry. A steady state conservation of energy was written for each of the zones, and then a standard form of the momentum equation was applied to the entire geometry to determine the draft. Agenbroad et al. [15] developed a model based on the Bernoulli equation that gives a simple expression for the volumetric flow rate of air through the chimney of a cookstove. This equation was solved simultaneously with the energy equation to determine the mass flow rate of air through the stove along with the temperature rise as functions of firepower.

A potential problem with RMHs is creating and sustaining adequate draft. The fluid flow resistance created by long lengths of ductwork, sinuous flow passages like the annular flow path between barrel and heat riser, and multiple fittings like elbows, tees (used for cleanouts), and dampers can cause “smoke-back.” Smoke back is an undesirable condition where the combustion gases meet too much flow resistance, causing them to travel back up into the room out of the burn chamber instead of through the ductwork and chimney.

A model that considers the fluid mechanics and heat transfer phenomena from a fundamental standpoint and accommodates geometric details and material properties particular to a RMH will be an invaluable tool for the designer. The model presented here is based on the differential form of the equations for one-dimensional analysis of conservation of mass, momentum, and energy, and predicts temperatures, pressures, and velocities throughout the system including the cob bench. Section 2 covers details of the model development; section 3 confirms the validity of the model through comparison with analytical solutions for a simplified problem and convergence studies, and presents and discusses results for a particular RMH geometry. Section 4 concludes the paper with a discussion of future model enhancements.

2. Model development

The model assumptions are as follows:

1. Unsteady thermal response of the mass is slow enough to warrant steady analysis of the fluid flow.
2. Flow is one dimensional.
3. Effects of fittings (elbows, tees, contractions and expansions, bends, logs, entrances, damper, etc.) and pipe friction are accounted for using standard expressions for fitting loss coefficients and the Moody friction factor.
4. Standard Nusselt number correlations are used for forced convection within the duct and natural convection away from the mass and exposed barrel and duct surfaces.
5. Radiation heat transfer is considered for the external heat transfer situations where natural convection occurs and across the gap between the duct and cob.
6. The surroundings are assumed to be at the same temperature as the room air.
7. Radiation is neglected in all internal flow passages.
8. The J-tube thermal mass is ignored.
9. Flows through the J-tube and the top section of the chimney are adiabatic.
10. The mass is geometrically simplified to a cylindrical mass of cob surrounding the horizontal duct section with the same

volume and length as the actual heater. The ends of the mass are insulated.

11. The unsteady cob temperature is assumed to vary in the flow and radial directions, but not azimuthally. A consequence of this assumption is that the boundary condition on the outside of the mass must be that of uniform convection and radiation to the room air and surroundings. This ignores the actual situation in which heat is conducted to the ground through the bottom of the mass.
12. Combustion gases have the same properties as air, which is assumed to behave as an ideal gas.
13. Combustion energy input is a point source at the beginning of the J-tube horizontal tunnel.

Fig. 2 shows the simplified geometry and coordinate system used for the model development, and Fig. 3 illustrates important dimensions for the model.

2.1. Derivation of the gas flow equations

The governing equations are written for the differential element shown in Fig. 4. In the figure, the quantity $\delta\dot{Q}_m$ is the rate of thermal energy production due to wood combustion (assumed only to occur in the element at the beginning the tunnel in the J-tube) and $d\dot{Q}_{out}$ is the heat loss through the differential surface area due to the temperature difference $T - T_{out}$. Note that the element shape and orientation indicated in Fig. 4 does not necessarily correspond to geometry in an actual RMH; the figure is intended to illustrate a general geometry that changes in cross-sectional area and elevation.

The heat loss can be expressed as

$$d\dot{Q}_{out} = UPds(T - T_{out}) \quad (1)$$

where U is the local overall heat transfer coefficient and P is the average perimeter of the element. Note that the value of T_{out} depends on the location in the gas flow path. For flow through the annular space between the barrel and the riser and through the uninsulated section of the chimney, T_{out} is equal to T_∞ (which is equal to the surrounding surfaces temperature T_{sur}). For flow through the horizontal duct in the cob mass, T_{out} is the mass inner surface temperature. For the insulated J-tube and insulated section of the chimney (where it passes through the ceiling, attic, and roof), $d\dot{Q}_{out} = 0$.

Accounting for pressure, body, and frictional forces on the element, it can be shown that the elemental momentum equation is [16]

$$dp + \rho VdV + \rho g dz + \rho \left(\frac{f}{D} ds + K_L \right) \frac{V^2}{2} = 0 \quad (2)$$

where f is the Moody friction factor, D is the hydraulic diameter, and K_L is a fitting loss coefficient. The first term represents net forces due to pressure, the second represents the change in momentum flow rate, the third represents body forces, and the last represents frictional forces due to wall shear stress and flow through fittings. A steady state energy balance on the element considering heat transfer and thermal, kinetic, and potential energy flow terms results in

$$\delta\dot{Q}_{in} = \dot{m}c_p dT + UP(T - T_{out})ds + \dot{m}(VdV + g dz) \quad (3)$$

where $c_p dT$ is the change in enthalpy across the element. The last term in Eq. (3) is typically negligible but is included here for completeness.

The final two equations describing the flow are the ideal gas equation:

$$p = \rho RT \quad (4)$$

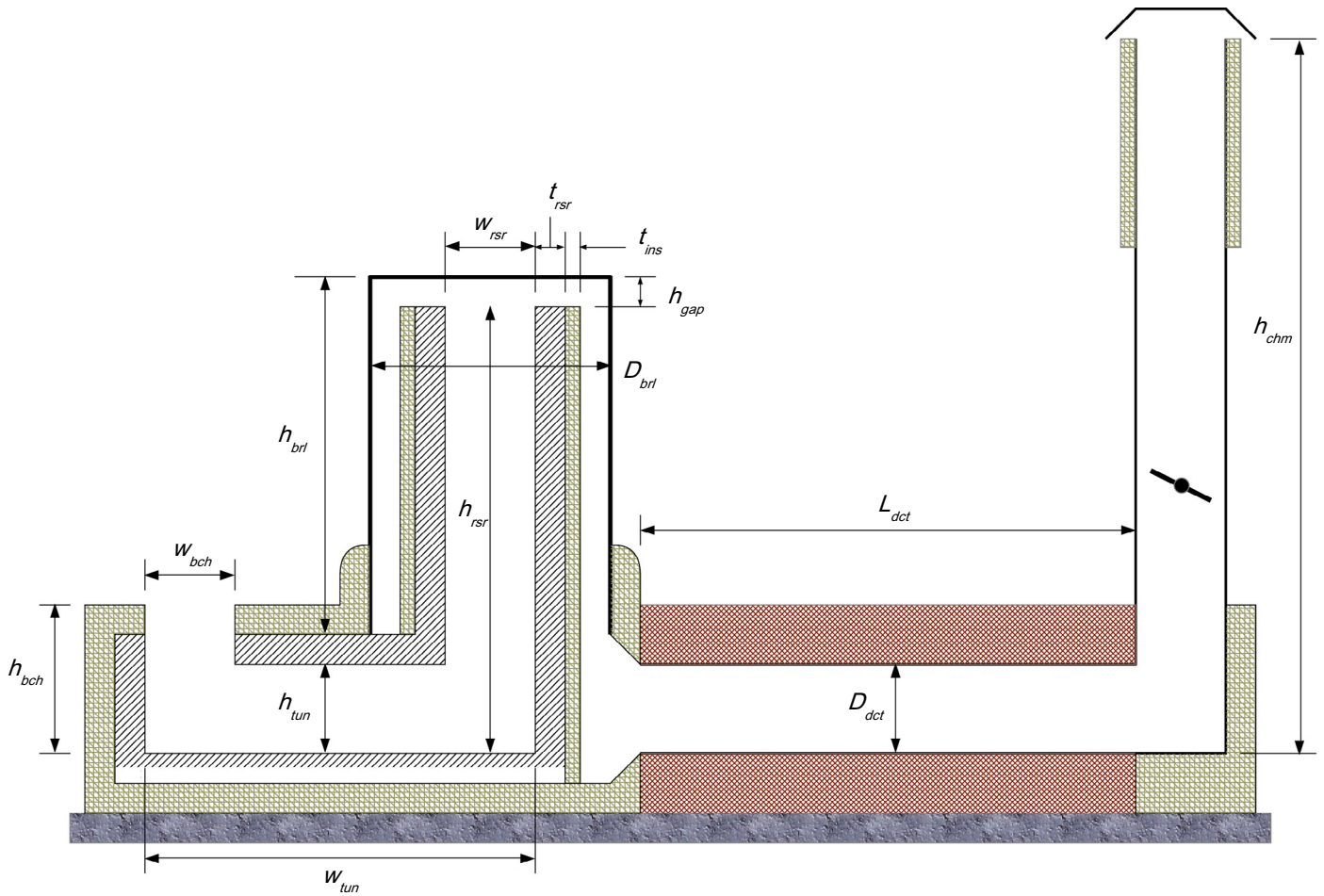


Fig. 3. Key dimensions. Not all dimensions are shown. For instance, the depth of the burn chamber, tunnel, and heat riser are perpendicular to the page.

and conservation of mass:

$$0 = \frac{d\rho}{\rho} + \frac{dA}{A} + \frac{dV}{V} \tag{5}$$

Eqs. (2)–(5) form a system of four equations for the four unknowns $V(s)$, $p(s)$, $T(s)$, and $\rho(s)$. The boundary conditions are known

pressure and temperature at the burn chamber inlet ($s=0$) and known pressure at the chimney exit. Note that there is no given boundary condition for velocity, as mass flow rate through the system is known only after a solution is obtained.

In order to solve for the flow variables numerically, the flow path through the heater is discretized into a series of N nodes, as indicated in Fig. 4. Since mass flow rate is an output of the

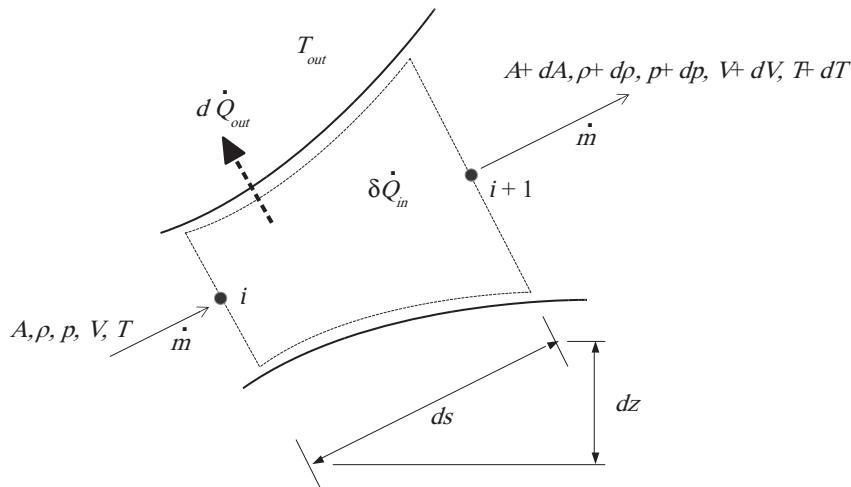


Fig. 4. The differential element used in the gas flow model. Also shown are nodes i and $i + 1$ used in the discretization process.

analysis, it is convenient to recast the conservation of mass, Eq. (5), as

$$\dot{m} = \rho VA = \text{constant} \quad (6)$$

Writing Eqs. (4) and (6) at node i gives

$$p_i = \rho_i RT_i \quad (7)$$

$$\dot{m} = \rho_i V_i A_i \quad (8)$$

Writing differentials as finite differences, Eqs. (2) and (3) become

$$(p_i - p_{i-1}) + \bar{\rho} \bar{V} (V_i - V_{i-1}) + \bar{\rho} g (z_i - z_{i-1}) + \bar{\rho} \left[\frac{f}{D} (s_i - s_{i-1}) + K_L \right] \frac{\bar{V}^2}{2} = 0 \quad (9)$$

$$\dot{Q}_{in} = \dot{m} c_p (T_i - T_{i-1}) + U \bar{P} (\bar{T} - T_{out}) (s_i - s_{i-1}) + \dot{m} [\bar{V} (V_i - V_{i-1}) + g (z_i - z_{i-1})] \quad (10)$$

where barred quantities are averages between values at nodes i and $i - 1$.

There are a total of $4N$ nodal values. Known inputs are T_i , p_i , and p_N , leaving $4N - 3$ unknowns. Recognizing that \dot{m} is also unknown, the number of unknowns increases to $4N - 2$. Eqs. (7)–(10) can be written for each of nodes for $2 \leq i \leq N$, and Eqs. (7) and (8) can be written at node 1, for a total of $4N - 2$ equations. The problem is thus fully determined.

The inlet pressure is determined from the following equation (see Appendix A).

$$p_i = p_N \exp \left[\frac{g}{R} \left(\frac{h}{T_{in}} + \frac{H-h}{T_{out}} \right) \right] \quad (11)$$

where H is the chimney height and h is the house height. T_{in} and T_{out} are the inside and outside house air temperatures.

The solution process begins by solving Eq. (7) for the density at node 1. The remaining system of nonlinear equations is solved using successive approximation beginning with initial guesses for the unknowns. Eq. (8) is solved for V_i . Eqs. (7)–(10) are rearranged to solve for ρ_i , V_i , p_i , and T_i respectively for $2 \leq i \leq N - 1$, where the right hand sides of these rearranged equations contain values at node $i - 1$ and previous iterates. At node N , Eqs. (7) and (10) are used to solve for ρ_N and T_N respectively, Eq. (9) is solved for V_N with known exit pressure p_N , and the mass flow rate is updated using Eq. (8). The iterations continue until the maximum change in all nodal values is less than a specified tolerance, ε (typically set equal to 1×10^{-3}). In practice the iterative solution process requires an underrelaxation of V_N before mass flow rate is updated:

$$V_N = V'_N + \omega (V_N - V'_N) \quad (12)$$

where V'_N is the previous iterate. A relaxation factor ω of 0.1 is suitable for most of the runs presented here, with lower values (0.05 or 0.01) necessary for marginal flow situations such as an almost closed damper or excessively small clearance between the barrel top and riser.

Determination of f , K_L , and U for various parts of the flow is discussed in section 2.3. A flowchart describing the solution algorithm is illustrated in Fig. 5.

The above procedure enables a solution for the gas flow properties for each time step. A boundary condition for the gas flow is the inner mass surface temperature as a function of position and time in the horizontal duct (T_{out} in Eq. 10). The determination of the unsteady mass temperature is considered in the next section.

2.2. Development of the equations for unsteady temperature distribution in the mass

The cob mass is modeled as a cylindrical wall of length L_{dct} with inside diameter D_i and outside diameter D_o (see Fig. 6). The inside diameter is set equal to the duct diameter. The outside diameter is determined by equating the actual cob volume, \forall , to the volume of the modeled cylinder:

$$D_o = \sqrt{\frac{4\forall}{\pi L} + D_i^2} \quad (13)$$

Assuming no temperature variation in the azimuthal direction, the governing differential equation is

$$\rho c_p \frac{\partial T_m}{\partial t} = k \left[\frac{1}{r} \frac{\partial}{\partial r} \left(r \frac{\partial T_m}{\partial r} \right) + \frac{\partial^2 T_m}{\partial x^2} \right] \quad (14)$$

with boundary conditions:

$$U_{in} [T(x) - T_m(r_i, x, t)] = -k \frac{\partial T_m}{\partial r}(r_i, x, t) \quad (15)$$

$$-k \frac{\partial T_m}{\partial r}(r_o, x, t) = U_{out} [T_m(r_o, x, t) - T_{\infty}] \quad (16)$$

$$\frac{\partial T_m}{\partial x}(r, 0, t) = \frac{\partial T_m}{\partial x}(r, L_{dct}, t) = 0 \quad (17)$$

and initial condition

$$T_m(r, x, 0) = T_{m_i} \quad (18)$$

Note that although the gas temperature $T(x)$ is not indicated explicitly as a function of time, it does in fact vary slowly in time according to the pseudo-transient treatment of gas/mass problem.

Eq. (14) is solved using a standard explicit finite difference method [17]. All boundaries and internal regions are discretized with second-order expressions in terms of nodal spacings Δx in the axial direction and Δr in the radial direction. Since the formulation is standard, only the resulting equation for an internal node and one of the boundary nodes is given here. The equation for the temperature at an internal node ij is

$$T_{m_{i,j}}^{p+1} = Fo_x (T_{m_{i-1,j}}^p + T_{m_{i+1,j}}^p) + Fo_r \left[\left(1 - \frac{1}{2} \frac{\Delta r}{r_j} \right) T_{m_{i,j-1}}^p + \left(1 + \frac{1}{2} \frac{\Delta r}{r_j} \right) T_{m_{i,j+1}}^p \right] + T_{m_{i,j}}^p [1 - 2(Fo_x + Fo_r)] \quad (19)$$

where superscript p signifies the time step number. The Fourier and Biot numbers are defined as

$$Fo_x = \frac{\alpha \Delta t}{\Delta x^2}$$

$$Fo_r = \frac{\alpha \Delta t}{\Delta r^2}$$

$$Bi = \frac{U \Delta r}{k_{mass}}$$

The gas and mass temperature solutions are linked through boundary condition (15) for the mass, where $T(x_i)$ is the local gas temperature and the value for T_{out} in Eq. (10) is the local mass inner surface temperature $T_m(r_i, x_i)$. Fig. 6 illustrates this linkage. Note that $\Delta s = \Delta x$ and that nodes for s correspond to the axial locations for x nodes. The finite difference equation for the mass boundary node corresponding to $T_m(r_i, x_i)$ is:

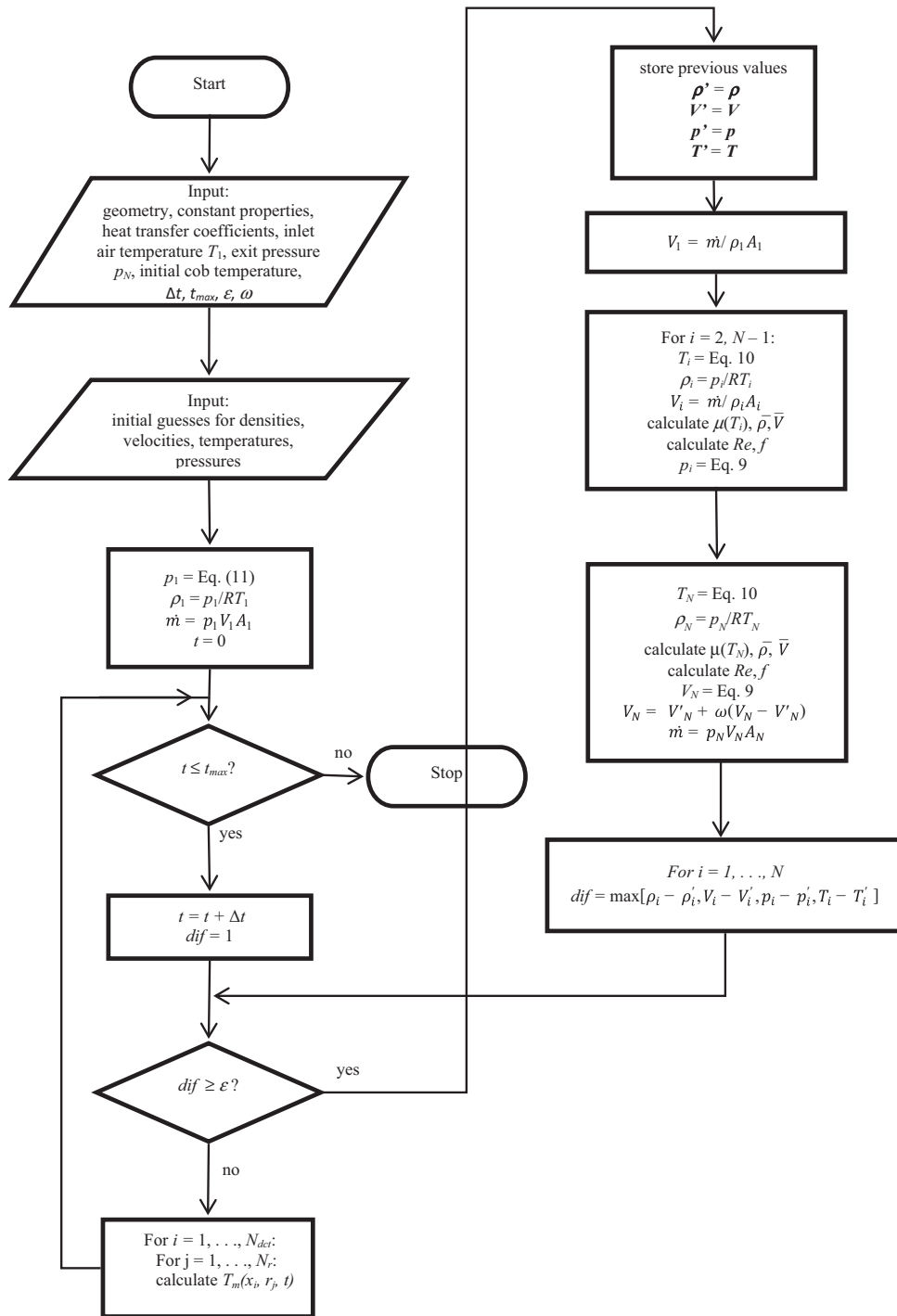


Fig. 5. Flowchart for the solution of the nonlinear equations in the model.

$$T_{m_{i,1}}^{p+1} = Fo_x (T_{m_{i-1,1}}^p + T_{m_{i+1,1}}^p) + 2Fo_r Bi T_i + 2Fo_r \left(1 + \frac{1}{2} \frac{\Delta r}{r_1}\right) T_{m_{i,j+1}}^p + T_{m_{i,j}}^p \left[1 - 2 \left(Fo_x + Fo_r \left(1 + \frac{1}{2} \frac{\Delta r}{r_1}\right) + Fo_r Bi\right)\right] \quad (20)$$

The temperature T_i in this equation is the local gas temperature. The explicit method has a time-step size limit based on the following criterion:

$$Fo_x + Fo_r \left(1 + \frac{1}{2} \frac{\Delta r}{r_1}\right) + Fo_r Bi \leq \frac{1}{2} \quad (21)$$

2.3. Friction factor, loss coefficients, and heat transfer coefficients

The friction factor f in Eq. (9) is calculated based on local Reynolds number:

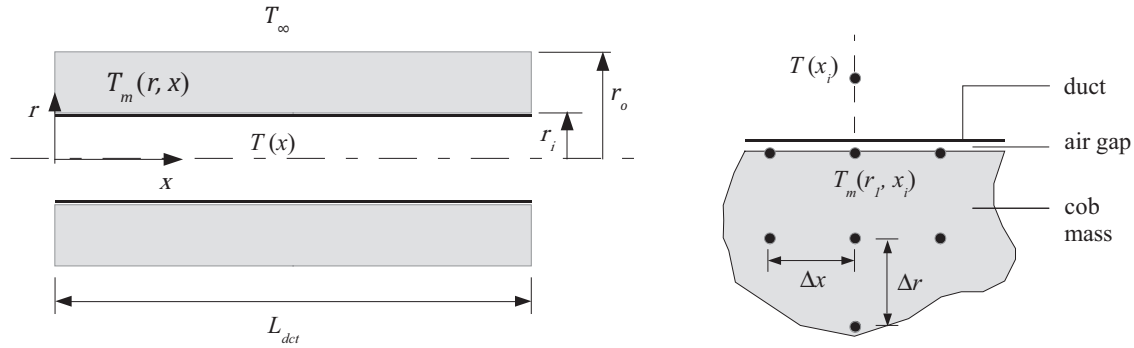


Fig. 6. The cob mass is modeled as a cylindrical wall with inner radius r_i , outer radius r_o , and length L_{dct} . T_m is the mass temperature, T is the gas temperature, and T_∞ is the surroundings and ambient air temperature. As shown on the right, the cob mass is discretized with uniform nodal spacings Δx in the flow direction and Δr in the radial direction.

$$f = \begin{cases} \frac{64}{Re} & Re \leq 2300 & (22) \\ 1.609 \times 10^{-8} Re^{1.856} & 2300 < Re < 3000 & (23) \\ (0.79 \ln Re - 1.64)^{-2} & 3000 \leq Re < 5 \times 10^6 & (24) \end{cases}$$

where the Reynolds number is based on the local average hydraulic diameter, average velocity, average density, and viscosity:

$$Re = \frac{\rho V D}{\mu}$$

The hydraulic diameter is determined from $D = 4A/P$, where A is the flow area and P is the perimeter. The first equation for f is from the analytical solution for laminar internal flow, the third is the Petukhov correlation for turbulent flows through smooth ducts [17], and the second is a logarithmic model derived by the author for the transitional range. The coefficient and exponent in Eq. (23) were determined by matching the values for f from Eq. (22) at $Re = 2300$ and Eq. (24) at $Re = 3000$.

The temperature dependence of viscosity is accounted for using the following relation

$$\mu = \frac{13.55 + 0.674T - 3.81 \times 10^{-4}T^2 + 1.183 \times 10^{-7}T^3}{10^7} \quad (25)$$

where T is in Kelvins and viscosity is in units of Ns/m^2 . This correlation is good for temperatures between 250 K and 1000 K and was

developed by the author by applying a polynomial curve fit to tabular data from Bergman et al. [17].

The correlation for f indicated above ignores surface roughness of the flow passages. Surface roughness is considered, however, for the flow past the logs. In this case, f is determined from the following equation [18]:

$$\frac{1}{\sqrt{f}} = -1.8 \log_{10} \left[\left(\frac{e/D}{3.7} \right)^{1.11} + \frac{6.9}{Re} \right] \quad (26)$$

The hydraulic diameter for the flow past the logs is determined from $D = 4A/P$, which for M logs of diameter d in a rectangular chamber of width w and depth h results in

$$D = \frac{4[wh - M\pi d^2/4]}{M\pi d + 2(w+h)} \quad (27)$$

Loss coefficients, K_L , for various flow regions within the RMH are shown in Table 1. The loss coefficient for the manifold transition from barrel exit to horizontal duct is assumed to be a sudden expansion.

The loss coefficient for the transition from riser to annular space between the barrel and riser deserves special attention. Referring to Fig. 7, the overall coefficient is assumed to be the sum of five components: miter bends from points 1 to a and b to 2, sudden expansions or contractions from 1 to a and b to 2, and fluid friction from a to b . The expression for the loss coefficient from 1 to 2 is thus

Table 1
Loss coefficients. Values are from Howell et al. [19]. Equations are from curve fits to tabular data in Howell et al. [19] unless otherwise noted.

Loss coefficient	Value or correlation	
K_{miter}	1.2	
K_{elbow}	0.37	
$K_{tee, straight thru}$	0	
$K_{tee, branch}$	1.1	
$K_{ent}: AR = (\text{percent open})/100$	0.5	$0.95 \leq AR \leq 1.0$
	$0.559AR^{-2.413} Re^{0.063}$	$0.2 \leq AR < 0.95$
$K_{sudden}: A_1$ is inlet area and A_2 is outlet area (Munson et al. [18])	$0.5 + 0.062 \frac{A_2}{A_1} - 1.337 \left(\frac{A_2}{A_1} \right)^2 + 0.899 \left(\frac{A_2}{A_1} \right)^3$	Contraction
	$\left(1 - \frac{A_1}{A_2} \right)^2$	Expansion
$K_{damper}: 0 < \theta < 80^\circ$, where $\theta = 0$ is fully open	$0.1502 + 0.0833 \theta + 0.004212 \theta^2 + 0.0001278 \theta^3$	

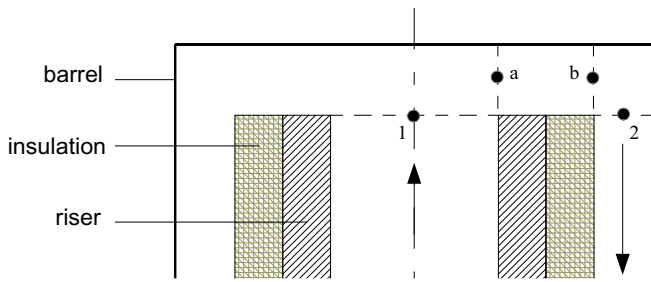


Fig. 7. Locations used in determining the loss coefficient for the riser-to-annulus transition.

$$K_{12} = \frac{K_{miter} \bar{V}_{1a}^2 + K_{sudden} \bar{V}_{max,1a}^2 + f_{ab} \frac{\Delta S_{ab}}{D_{ab}} + K_{miter} \bar{V}_{b2}^2 + K_{sudden} \bar{V}_{max,b2}^2}{\bar{V}_{12}^2} \quad (28)$$

where \bar{V}_{ij} indicates the average speed between points i and j , and $\bar{V}_{max,ij}$ indicates the maximum speed between the flow areas corresponding to points i and j . The friction factor f_{ab} is based on the average speed \bar{V}_{ab} and D_{ab} is the average hydraulic diameter between points a and b . Values for K_{miter} and K_{sudden} are given in Table 1.

Values for overall heat transfer coefficients, U , in Eqs. (10), (15), and (16) are determined as follows. For the barrel top, barrel sides (annulus), and chimney sides

$$U = \frac{1}{\frac{1}{h_{ci}} + \frac{t}{k} + \frac{1}{h_{co} + h_r}} \quad (29)$$

where h_{ci} is determined from the Dittus–Boelter Nusselt number relationship and h_{co} is determined from appropriate natural convection relationships listed in Table 2. The term t/k is the conduction resistance for the barrel or chimney walls, and the radiation heat transfer coefficient h_r is determined from

$$h_r = \epsilon \sigma (T_s + T_{sur})(T_s^2 + T_{sur}^2) \quad (30)$$

For the inside barrel top, where the rising combustion gases strike the barrel top and are redirected into the annular space between barrel and riser, the following correlation for an impinging jet is used [17]:

$$Nu = G \left[2Re^{0.5} (1 + 0.005Re^{0.55})^{0.5} \right] Pr^{0.42} \quad (31)$$

where

$$G = 2A_r^{0.5} \frac{1 - 2.2A_r^{0.5}}{1 + 0.2(H/D - 6)A_r^{0.5}} \quad (32)$$

and

$$A_r = \frac{D^2}{4R^2} \quad (33)$$

In these relationships D is the hydraulic diameter of the riser and R is the barrel radius. The jet length, H , is equal to the gap height between the riser exit and barrel inside surface. It should be noted that the expression for Nu is only a rough approximation for the convection in this area. The expression is valid for H/D ratios between about 2 and 12, whereas for the RMH modeled in section 3 the H/D ratio is 0.27. Also, the expression is valid for an external impinging jet flow, whereas the current flow is internal. Given the lack of relevant published correlations, and noting that the calculated values for h using this equation are similar in value to internal flow convection coefficients calculated for other flow passages in the geometry, the use of the correlation is justified.

Natural convection correlations are based on the Rayleigh number:

$$Ra = \frac{g\beta(T_s - T_\infty)L^3}{\alpha\nu} \quad (34)$$

where T_s is the average surface temperature, T_∞ is the air temperature, L is the characteristic length, and β is the volumetric thermal expansion coefficient, which is the inverse of the film temperature expressed in absolute units (the film temperature is the average of the surface and ambient temperatures).

The overall heat transfer coefficients appearing as boundary conditions for the mass in Eqs. (15) and (16) are specified as follows. For U_{in} , a small gap is assumed to exist between the outside duct and inside cob surface (due to contraction of the cob as it cures, or construction defects). The heat transfer into the cob at $r = r_i$ thus considers convection from the gas to the duct inside surface, conduction through the duct wall, and conduction and radiation through the air gap. The expression for U_{in} is thus

$$U_{in} = \left[\frac{1}{h_{ci}} + \frac{t_{dct}}{k_{dct}} + \frac{1}{\frac{k_{gap}}{t_{gap}} + h_r} \right]^{-1} \quad (35)$$

where t_{dct} and k_{dct} are the duct thickness and thermal conductivity, and t_{gap} and k_{gap} are the air space thickness and thermal conductivity. The radiation heat transfer coefficient for the gap, h_r , is found from the expression for that between two parallel planes:

$$h_r = \frac{\sigma(T_1 + T_2)(T_1^2 + T_2^2)}{\frac{2}{\epsilon} - 1} \quad (36)$$

Table 2

Nusselt number correlations used to determine h , from Bergman et al. [17].

Convection type and location	$Nu (=hD/k) =$	Length scale for Re , Ra , and Nu
Forced internal flows except barrel top	$0.023Re^{0.8}Pr^{0.3}$	$4A/P$
Forced inside barrel top	Eq. (31)	
Natural external barrel top	$0.54 Ra^{0.25}$	$D_{brl}/4$
Natural external barrel sides	$\left\{ 0.825 + \frac{0.387Ra^{1/6}}{\left[1 + (0.492/Pr)^{9/16} \right]^{8/27}} \right\}^2$	Barrel height
Natural external mass	$\left\{ 0.60 + \frac{0.387Ra^{1/6}}{\left[1 + (0.559/Pr)^{9/16} \right]^{8/27}} \right\}^2$	Mass diameter

where ε is the emissivity of the surfaces on either side of the gap (both the duct outer and cob inner surface are assumed to have the same emissivity), and T_1 and T_2 are the gap surface temperatures.

The outside overall heat transfer coefficient is determined from $U_{out} = h_{co} + h_r$, where h_{co} and h_r are the convection and radiation heat transfer coefficients for the mass outer surface.

Heat transfer coefficients, like the friction factor f , are dependent on flow velocities and temperatures which vary both spatially and temporally, and are dependent on model inputs such as \dot{Q}_{in} . Unlike f , however, the current model is set up to input constant values for convection coefficients h rather than calculating values as part of the solution process. The input values are calculated based on approximate expected velocities and temperatures. Future versions of the model will account for velocity and temperature variations, although experience shows that results for mass flow rate and efficiency are not significantly affected by changes in convection and radiation coefficients due to variations in velocities and temperatures across typical ranges.

2.4. Model outputs

The model outputs air density, velocity, pressure, and temperature as function of s and time, the cob mass temperature as a function of space and time, and the mass flow rate of air as a function of time. Also of interest is the system efficiency. The instantaneous efficiency is defined as the rate of heat transfer from the gas flow to the room divided by the rate of heat input:

$$\eta = \frac{\dot{m}c_p(T_{max} - T_{min})}{\dot{Q}_{in}} \quad (37)$$

In this equation, T_{max} is the air temperature at the node just downstream node at which \dot{Q}_{in} occurs, and T_{min} is the temperature of the gas leaving the chimney. Overall efficiency for the burn duration of $0 \leq t \leq t_{max}$ is

$$\bar{\eta} = \frac{1}{t_{max}} \int_0^{t_{max}} \eta dt \quad (38)$$

which is simply a time-averaged efficiency.

2.5. Analytical solution for a simple chimney

The model is tested using an analytical solution for a vertical constant-diameter adiabatic chimney of height h including fluid friction (see Fig. A1). Combustion is modeled as a point heat addition just upstream of the inlet, where the temperature is specified as T_{in} . For the adiabatic case, neglecting kinetic and potential energy terms, the energy equation shows that temperature remains constant in the chimney from the inlet to exit. The temperature of the air outside the chimney is T_{out} . The inlet to exit pressure ratio can be expressed as (see Appendix A):

$$\frac{p_1}{p_2} = \exp\left(\frac{gh}{RT_{out}}\right) \quad (39)$$

The continuity, momentum, and ideal gas equations can be combined and solved to give the following expression for chimney inlet velocity (see Appendix B for details):

$$V_1 = \sqrt{\frac{2gh\left(\frac{T_{in} - T_{out}}{T_{out}}\right)}{\left(\frac{p_1}{p_2}\right)^2 - 1 + \frac{fh}{4D}\left(1 + \frac{p_1}{p_2}\right)^2}} \quad (40)$$

where the friction factor f is assumed to be constant along the entire chimney.

3. Results and discussion

3.1. Simple vertical chimney

Results for the model applied to a simple vertical adiabatic chimney compare well with the analytical solution given in Eq. (40). For inputs $h = 7$ m, chimney diameter = 0.1 m, $T_{in} = 500$ K, $T_{out} = 300$ K, $p_2 = 101,300$ Pa, $c_p = 1000$ J/kg K, $g = 9.81$ m/s², $R = 287$ J/kg K, and $f = 0$, the solution for the inlet velocity is 239.5 m/s. The error in the computational solution, which is essentially independent of number of nodes because the solutions for density, velocity, and pressure are linear with respect to z , is 0.26%. For $f = 0.05$, the analytical solution for the inlet velocity is 5.111 m/s, and the computational solution has an error of 0.0016%. If the chimney is nonadiabatic, heat loss results in nonlinear changes in the flow variables with respect to elevation. The solution now is sensitive to the number of nodes, N , but there is no available analytical solution for comparison. Instead, solutions with $U = 50$ W/m² K for increasing values of N were compared to a high-resolution solution with $N = 1001$. The results showed smooth convergence towards the high-resolution solution, with an error of 0.12 percent for $N = 3$ and an error of 1.6×10^{-4} percent for $N = 51$.

3.2. Results for the model RMH

Results are presented for a RMH with thermal and geometric inputs listed in Table 3. Table 4 lists the values of h used for the results presented. The burn duration for most results shown is five hours. For a five-hour burn, a total of 225 nodes, and a time step size of 100 s, the run time on a desktop PC is about 4 seconds. Note that the value of 13,500 W for \dot{Q}_{in} was determined by using a wood heating value of 17 MJ/kg [20] and a feed rate of 2.85 kg/h.

A numerical model can be validated by showing convergence to a constant solution as time step size and nodal spacing are decreased. Fig. 8 shows that as the time step size decreases the solution for overall efficiency converges smoothly to constant value. Fig. 9 shows the similarity of the pressure solution for a coarse ($N = 150$) and fine ($N = 3000$) resolution, indicating that the solution is not strongly dependent on the number of nodes. Given these demonstrations of the model's spatial and temporal convergence properties, subsequent results are given for $N = 225$ and $\Delta t = 100$ s. The number of nodes in various sections of the RMH is as follows: 9 in the burn chamber, 9 in the tunnel, 21 in the riser, 15 in the annulus, 63 in the duct, and 108 in the chimney.

Fig. 9 shows how the elevation, pressure, and temperature change throughout the system as functions of s . The pressure shows the expected behavior of decreasing with distance due to frictional effects, and fluctuations due to increases or decreases in elevation. As seen on the figure, the temperature remains constant through the insulated sections, and changes across other parts of the system as shown. The highest temperature, which occurs at the point of heat input in the beginning of the tunnel, remaining constant until the top of the riser, is 518 K. Considering the thermal resistance due to the inside convection, conduction through the barrel, and convection plus radiation on the barrel top external surface, the temperature of the outside surface of the barrel top can be calculated to be 408 K, or 135 °C.

Fig. 10 shows how the mass temperature varies in the radial and flow directions. Note that the cob inner surface temperature at the duct inlet is 393 K, almost 100 K less than the gas temperature at that point. This demonstrates the importance of good thermal contact between cob and duct. For this case, the air gap is 1 mm. If we decrease the air gap to 0.1 mm, the maximum cob temperature becomes 402 K, and if we increase it to 5 mm, the max temperature decreases to 379 K.

Table 3
Thermal and geometric properties for the RMH.

Parameter	Value	Units
Thermal conductivities		
Steel (barrel, duct, and chimney)	50	W/m K
Cob	0.524	
Thermal diffusivity for cob		
	3.5e-7	m ² /s
Temperatures		
Inside air	288	K
Outside air	273	
Surroundings	288	
Chimney exit pressure	101,300	Pa
Rate of heat input from combustion	13,500	W
Thicknesses		
Barrel thickness	1.22 × 10 ⁻³	m
Duct thickness	5.59 × 10 ⁻⁴	
Riser thickness	0.03175	
Riser insulation thickness	0.03175	
Airgap between cob and duct	1 × 10 ⁻³	
J-tube dimensions		
Burn chamber height, <i>h_{bch}</i>	0.4064	
Burn chamber width, <i>w_{bch}</i>	0.1778	
Burn chamber depth	0.1905	
Tunnel height, <i>h_{tun}</i>	0.1778	
Tunnel width, <i>w_{tun}</i>	0.6096	
Tunnel depth	0.1905	
Riser height, <i>h_{rsr}</i>	1.2192	
Riser depth	0.1905	
Riser width, <i>w_{rsr}</i>	0.1778	
Barrel/riser gap, <i>h_{gap}</i>	0.05	
Barrel diameter, <i>D_{brl}</i>	0.584	
Barrel height, <i>h_{brl}</i>	0.762	
Duct diameter, <i>D_{dct}</i>	0.2032	
Duct length, <i>L_{dct}</i>	4.0	
Total chimney height, <i>h_{chm}</i>	7.0	
Insulated chimney height	5.0	
House height	6.0	
Cob volume	1.36	m ³
Number of elbows	2	
Number of straight flow through tees	2	
Number of branch flow tees	2	
Log dimensions		
Diameter	0.065	m
Length	0.3	
Roughness	0.0009	
Number of logs, <i>M</i>	6	
Elbow locations (<i>x</i>)	1.0, <i>L_{dct}</i> - 1.0	m
Branch tee locations (<i>x</i>)	2.0, <i>L_{dct}</i> - 2.0	m

Table 4
Numerical values for convection and radiation coefficients.

	Value, W/m ² K
Convection coefficient, <i>h_c</i>	
Inside barrel top	15.6
Outside barrel top	7.2
Annulus	3.4
Outside barrel side	4.8
Inside duct	9.1
Inside chimney	10.5
Outside mass	1.9
Outside chimney	5.0
Radiation coefficient, <i>h_r</i>	
Outside barrel top	7.2
Outside barrel side	5.9
Outside chimney	6.4
Between duct and inner mass surface	9.3
Outside mass	5.0

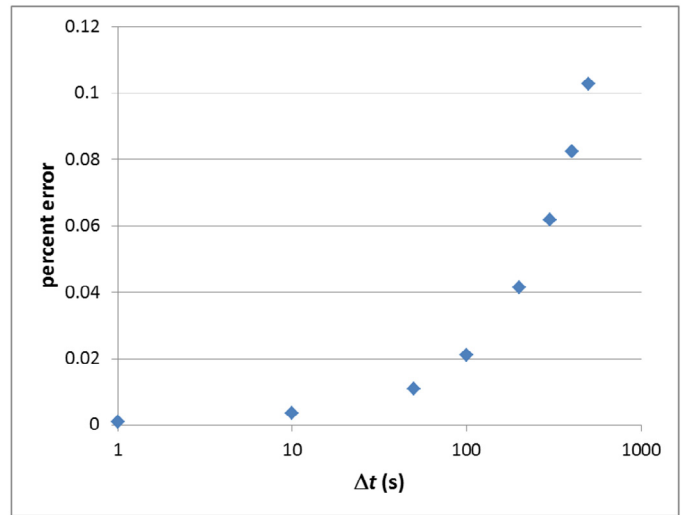


Fig. 8. Percent error as a function of time step size. Percent error is $100(x_{\Delta t} - x_{0.1})/x_{0.1}$, where $x_{0.1}$ is the overall efficiency for a five-hour burn with $\Delta t = 0.1$ s ($\bar{\eta} = 0.37918$).

Of particular interest is the cool down period of the mass. Fig. 11 shows the average mass outside surface temperature for a 5 hour burn and subsequent cool down period of 15 hours. The figure clearly shows how the thermal energy continues to work its way through the mass after combustion stops, causing a peak surface temperature at about 10 hours into the transient. At the end of the 20 hour transient, the RMH is still producing a draft of 0.016 kg/s, down from a value of 0.058 kg/s just before the end of the burn. Also shown on the figure is the mass flow rate for the case where the damper is left fully open for the entire transient (in practice, the damper would typically be closed to contain heat). A sharp decrease is apparent when the heat source is extinguished, after which the draft diminishes as the mass cools asymptotically to room temperature.

A rule of thumb for RMH design is that the flow area should at no point be less than the burn chamber inlet area. Of particular concern is the area corresponding to the gap at the top of the barrel, where the flow transitions from the riser to the annular space (this dimension is not easy to control during a typical RMH construction). For the current configuration where the gap height is 50 mm, the associated flow area is 0.037 m², while the burn chamber inlet area is 0.034 m², which satisfies the rule of thumb. The gas mass flow rate in this case is 0.058 kg/s. If the gap height is decreased to 25 mm, the mass flow rate decreases by ten percent to 0.052 kg/s. If the gap is further decreased to only 10 mm, the mass flow rate diminishes by 47% to 0.031 kg/s. Fig. 12 clearly shows that for 10 mm, the gap becomes the dominant loss.

Chimney height plays an important role in producing adequate draft. Fig. 12 shows how the pressure is affected by decreasing the chimney height to 2 meters, and eliminating insulation. The mass flow rate substantially decreases to 0.026 kg/s, a 55% decrease from a chimney height of 7 m. The overall driving pressure gradient is substantially less, and the adverse pressure rise in the annulus becomes a significant portion of the total pressure drop from inlet to exit. It should be noted that the maximum temperature for this case is 808 K, which is almost 300 degrees greater than the base case. This means substantial temperatures must be developed in the burn chamber to produce a draft. In all likelihood, the value of 13.5 kW for \dot{Q}_m would not be attainable with this geometry.

A damper in the system can serve to restrict the flow of exhaust gases and thus decrease the amount of heat that is lost through the chimney exit. Fig. 13 shows how the overall efficiency increases with

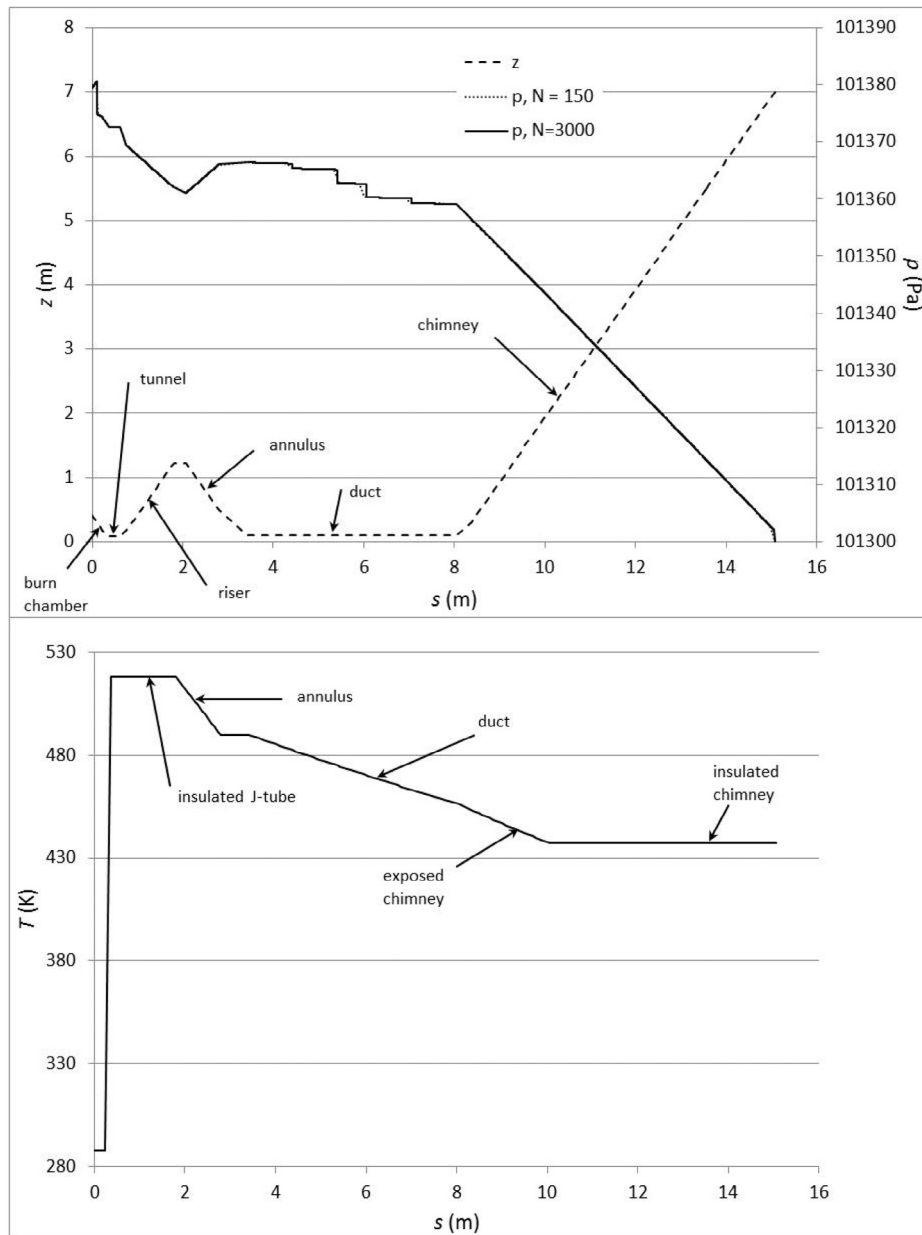


Fig. 9. Elevation, pressure, and temperature as functions of distance along the flow path. Pressure solutions for coarse ($N = 150$) and fine ($N = 3000$) grids are shown in order to demonstrate the insensitivity of the solution to the number of nodes. Note that the pressure decreases sharply through the logs and in the branch tees, and rises in the annulus as the elevation decreases. The sudden temperature rise due to the point heat input can be seen on the left of the lower plot, where temperature through other parts of the system is also indicated.

increasing damper angle (zero degrees corresponds to fully open), along with the diminishing mass flow rate.

As a final test the length of the duct and cob is increased to determine the effect on overall efficiency of the RMH due to more heat from the gas being absorbed by the mass prior to the gas exiting through the chimney. Doubling the length from 4 m to 8 m increases the efficiency significantly from 38% to 51%. A question that arises is: what is the maximum length of duct that could be used without impeding the draft potential? In order to answer this question, a criterion would have to be developed to identify configurations which are unlikely to result in adequate combustion. Only a more sophisticated heat input model considering combustion physics will help to answer this question, as addressed in the next section.

4. Conclusions and future work

Many model enhancements are possible. A more robust non-linear equation solver will eliminate the need for the trial-and-error approach required to find an appropriate relaxation factor for the successive approximation solution procedure. Also, the inclusion of functions for the calculation of velocity- and time-dependent heat transfer coefficients will avoid the need for pre-calculation and input of these values, and should result in more accurate predictions. In the current model the gas flow through the J-tube is adiabatic, but in reality the firebrick forming the J-tube wall absorbs heat from the gases until equilibrium temperatures are reached. Modeling this will entail an unsteady treatment of the J-tube similar to that currently used for the cob mass. The current model ignores

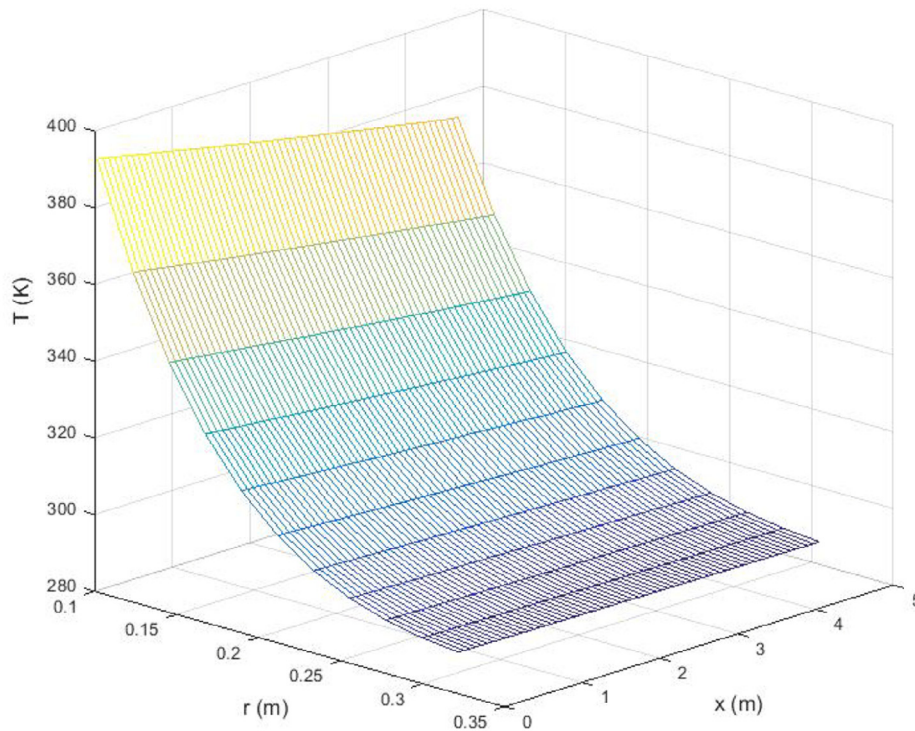


Fig. 10. Temperature of the mass at the end of a five hour burn. The figure shows how the inside surface temperature decreases slightly in the direction of fluid flow, and the significant temperature gradients in the radial direction.

the conduction heat transfer through the bottom of the mass into the ground. To account for this boundary condition a three-dimensional model would be necessary. Results show, however, that axial variations in temperature are small, so a two-dimensional discretization may still be reasonable, with variations occurring in the radial and azimuthal directions. A diversity of boundary conditions could then be applied on the perimeter of the mass.

The model now takes as an input the firepower \dot{Q}_m , but this is not a factor entirely controllable by the user. For instance, if the user increases the damper angle, the mass flow rate of air decreases, which in turn decreases the burn rate. A more thorough modeling of combustion physics must be undertaken to understand the conditions (limiting values of duct diameter and length, chimney height, barrel gap height, annulus area, etc.) under which combustion

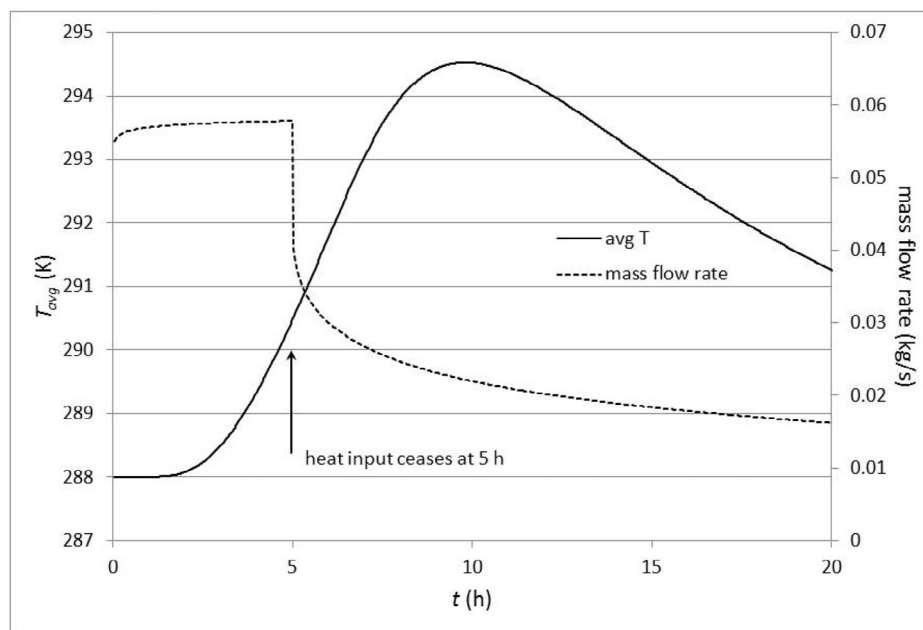


Fig. 11. The average mass outside surface temperature as a function of time. The fire is extinguished at $t = 5$ hours. At 20 hours, the mass is still releasing heat into the room. The peak mass temperature occurs at about 10 hours, at 21 °C, six degrees warmer than the ambient.

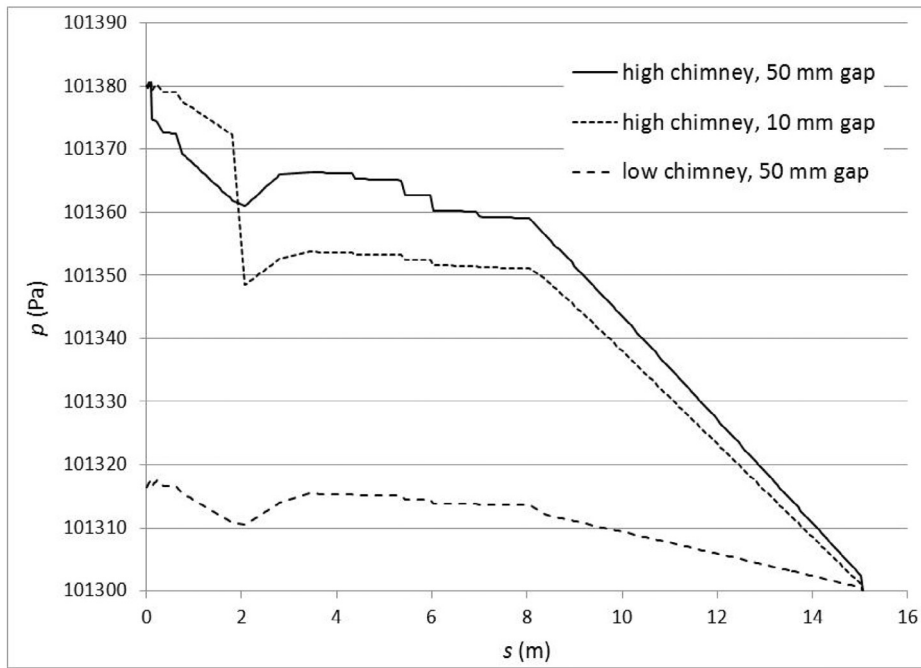


Fig. 12. The effect of gap height between riser and barrel top and chimney height on spatial pressure variation. The high chimney is 7 m and the low chimney is 2 m.

becomes unsustainable, or under which a proper draft is unattainable.

The proposed compressible flow model provides a fast, reasonable demonstration of how RMH performance is influenced by changes in various inputs. Of course, a more rigorous model using Computational Fluid Dynamics (CFD) software may provide more realistic results, but this option is only accessible to CFD specialists willing to invest the time and effort required for three-dimensional mesh creation and other modeling details. The algorithm, which is relatively simple to program, provides quick results and allows straightforward adjustments to account for

geometry changes and other inputs. Its simplicity also makes it suitable for a web-based calculation tool that could be developed for use by nontechnical users interested in RMH design.

The model compares well with analytical solutions to a simplified geometry and shows convergence in both time and space. What is still lacking, however, is a rigorous comparison with actual RMH thermal measurements. This comparison will allow necessary adjustments to loss and heat transfer coefficients or other model aspects to bring the results in line with reality. Once the model is validated in this way, it will become a useful design tool for the RMH community.

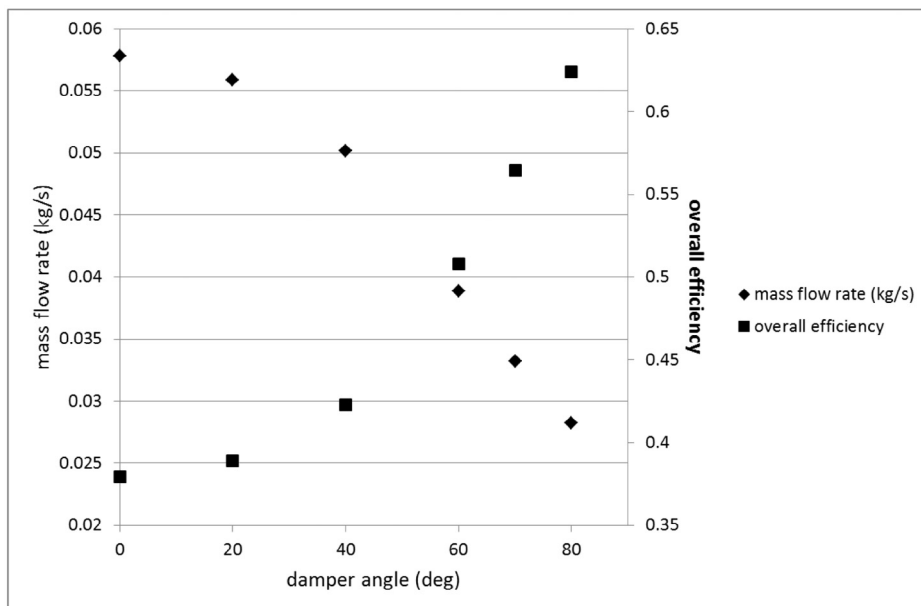


Fig. 13. Mass flow rate and overall efficiency as functions of damper angle.

Appendix A

Derivation of the equation for inlet pressure.

We are interested in deriving the expression that relates the exterior pressure at the chimney exit, p_2 , to the pressure at the inlet to the chimney (or burn chamber), $p_{1,i}$. See Fig. A1.

The inside and outside temperatures T_{in} and T_{out} are assumed to be constant. The house height is h , and the chimney height is H . We assume that the neutral pressure level for the house is at point 3, so $p_{3,o} = p_{3,i} = p_3$. Using the expression for pressure variation with elevation z in a stagnant fluid, $dp = -\rho g dz$, along with the ideal gas equation, $\rho = p/RT$, gives $dp/p = -g/RT dz$. Integrating between the points corresponding to $p_{1,o}$ and p_2 and solving for $p_2/p_{1,o}$ gives

$$\frac{p_2}{p_{1,o}} = \exp\left(-\frac{gH}{RT_{out}}\right) \quad (A1)$$

Likewise, integrating between points 1,i and 3,i leads to

$$\frac{p_3}{p_{1,i}} = \exp\left(-\frac{gh}{RT_{in}}\right) \quad (A2)$$

and integrating between 1,o and 3,o gives

$$\frac{p_3}{p_{1,o}} = \exp\left(-\frac{gh}{RT_{out}}\right) \quad (A3)$$

Combining these three pressure ratios leads to the following relationship:

$$\frac{p_{1,i}}{p_2} = \exp\left[\frac{g}{R}\left(\frac{h}{T_{in}} + \frac{H-h}{T_{out}}\right)\right] \quad (A4)$$

The argument for the exponential is small, typically on the order of 1×10^{-3} . The first two terms of the series expansion for an exponential can thus be applied, leading to

$$p_{1,i} = p_2 \left[1 + \frac{g}{R} \left(\frac{h}{T_{in}} + \frac{H-h}{T_{out}} \right) \right] \quad (A5)$$

Note that occasionally it is claimed that for an RMH the chimney height H can be less than house height h . In this case the last term in the equation serves to decrease the overall driving pressure force, resulting in a possibly significant decrease in draft potential.

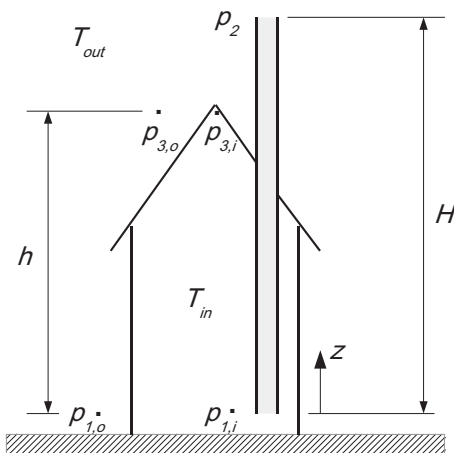


Fig. A1.

Appendix B

Derivation of the equation for mass flow rate in a simple vertical adiabatic chimney with a point heat source just upstream of the inlet.

We analyze a vertical chimney of height h and constant diameter D . See Fig. B1.

Assuming that the chimney is adiabatic and mechanical energy terms in the energy equation can be neglected, the temperature throughout the chimney is $T = T_{in}$. The continuity, ideal gas, and momentum equations are [16]:

$$\frac{dV}{V} + \frac{d\rho}{\rho} = 0 \quad (B1)$$

$$p = \rho RT \quad (B2)$$

$$dp + \rho V dV + \rho g dz + \rho \frac{V^2}{2} \frac{fdz}{D} = 0 \quad (B3)$$

For $T = \text{constant}$, Eq. (B2) gives $dp = RT d\rho$. Substituting this into Eq. (B3) and dividing by density gives

$$RT \frac{d\rho}{\rho} + V dV + g dz + \frac{V^2}{2} \frac{fdz}{D} = 0 \quad (B4)$$

Using Eq. (B1) to substitute for $d\rho/\rho$ leads to

$$-RT \frac{dV}{V} + V dV + g dz + \frac{V^2}{2} \frac{fdz}{D} = 0 \quad (B5)$$

We now assume that the friction factor is constant, and that V in the fourth term can be assumed to be constant with a value of $\bar{V} = (V_1 + V_2)/2$, so that Eq. (B5) can be integrated from $z = 0$ (point 1) to $z = h$ (point 2) to give:

$$-RT \ln\left(\frac{V_2}{V_1}\right) + \frac{1}{2}(V_2^2 - V_1^2) + gh + \frac{fh}{2D} \left(\frac{V_1 + V_2}{2}\right)^2 = 0 \quad (B6)$$

Combining the continuity equation $\rho_1 V_1 = \rho_2 V_2$ and the ideal gas equation for constant temperature $p_1/\rho_1 = p_2/\rho_2$ to eliminate density gives $V_2/V_1 = p_1/p_2$. Eq. (B6) can then be solved for V_1 in terms of the pressure ratio p_1/p_2 :

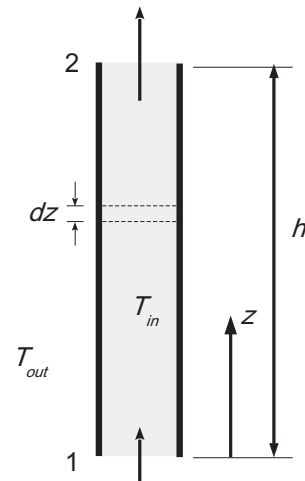


Fig. B1.

$$V_1 = \sqrt{2 \frac{RT \ln \left(\frac{p_1}{p_2} \right) - gh}{\left(\frac{p_1}{p_2} \right)^2 - 1 + \frac{fh}{D} \frac{1}{4} \left(1 + \frac{p_1}{p_2} \right)^2}} \quad (\text{B7})$$

The pressure ratio can be expressed as (see Appendix A):

$$\frac{p_1}{p_2} = \exp \left(\frac{gh}{RT_{out}} \right) \quad (\text{B8})$$

Recalling that $T = T_{in}$, Eqs. (B7) and (B8) can be combined to give

$$V_1 = \sqrt{\frac{2gh \left(\frac{T_{in} - T_{out}}{T_{out}} \right)}{\left(\frac{p_1}{p_2} \right)^2 - 1 + \frac{fh}{4D} \left(1 + \frac{p_1}{p_2} \right)^2}} \quad (\text{B9})$$

Several observations can be made regarding Eq. (B9). The argument for the exponential in Eq. (B8) is small (on the order of 1×10^{-3}). The exponential term can thus be approximated as the first two terms in the series expansion for e : $\exp(\varepsilon) \cong 1 + \varepsilon$, where $\varepsilon = gh/RT_{out}$, so p_1/p_2 can be substituted with $1 + \varepsilon$ and Eq. (B9) becomes

$$V_1 = \sqrt{\frac{2gh \left(\frac{T_{in} - T_{out}}{T_{out}} \right)}{(1 + \varepsilon)^2 - 1 + \frac{fh}{4D} (2 + \varepsilon)^2}} \quad (\text{B10})$$

Expanding the denominator of Eq. (B10) and neglecting ε^2 terms gives

$$V_1 = \sqrt{\frac{2gh \left(\frac{T_{in} - T_{out}}{T_{out}} \right)}{2\varepsilon + \frac{fh}{D} (1 + \varepsilon)}} \quad (\text{B11})$$

Two cases can be observed. Setting $f = 0$ and substituting for ε leads to

$$V_1 = \sqrt{R(T_{in} - T_{out})} \quad (\text{B12})$$

This equation indicates that for frictionless flow, the velocity depends only on the inside and outside temperatures and not the chimney height.

For nonzero f , if we assume fh/D is $O(1)$, Eq. (B11) is simplified to

$$V_1 = \sqrt{\frac{2gD}{f} \left(\frac{T_{in} - T_{out}}{T_{out}} \right)} \quad (\text{B13})$$

where, again, the solution for velocity is independent of h . If instead we write f as a loss coefficient based on the chimney height:

$$K_L = \frac{fh}{D} \quad (\text{B14})$$

the expression for V_1 becomes

$$V_1 = \sqrt{\frac{2gh}{K_L} \left(\frac{T_{in} - T_{out}}{T_{out}} \right)} \quad (\text{B15})$$

Multiplying by area gives the volumetric flow rate:

$$\dot{V}_1 = A \sqrt{\frac{2gh}{K_L} \left(\frac{T_{in} - T_{out}}{T_{out}} \right)} \quad (\text{B16})$$

Eq. (B16) is similar to Agenbrood's expression for chimney flow rate [15], except the quantity $1/\sqrt{K_L}$ replaces Agenbrood's loss coefficient, C . It should be noted that the frictionless case ($K_L = 0$) cannot be accounted for using this equation. The proper equation for frictionless flow is Eq. (B12).

Nomenclature

A	area
Bi	Biot number
c_p	specific heat
D	hydraulic diameter
e	relative roughness
f	friction factor
FO	Fourier number
g	acceleration due to gravity
h	house height
h_{ci}	inside convection coefficient
h_{co}	outside convection coefficient
h_r	radiation heat transfer coefficient
H	chimney height
k	thermal conductivity
K	loss coefficient
L_{det}	duct length
\dot{m}	mass flow rate
N	total number of nodes
Nu	Nusselt number
p	pressure
P	perimeter
Pr	Prandtl number
r	radial coordinate
R	ideal gas constant
Ra	Rayleigh number
Re	Reynolds number
\dot{Q}	heat transfer rate
s	gas flow path coordinate, $s = 0$ at burn chamber inlet
t	time or thickness
T	gas temperature
T_{in}	inside temperature
T_m	mass temperature
T_{out}	outside temperature
T_s	surface temperature
T_{sur}	surroundings temperature
T_∞	air temperature
U	overall heat transfer coefficient
V	speed
x	gas flow path coordinate, $x = 0$ at duct inlet
z	elevation

Symbols

α	thermal diffusivity
β	volumetric thermal expansion coefficient
ε	emissivity or tolerance
η	efficiency
μ	absolute viscosity
ν	kinematic viscosity
ρ	density
\forall	volume
σ	Stefan–Boltzmann constant
ω	relaxation factor

References

- [1] [K.B. Sutar, S. Kohli, M.R. Ravi, A. Ray, Biomass cookstoves: a review of technical aspects, Renew. Sustain. Energy Rev. 41 \(2015\) 1128–1166.](#)

- [2] [M. Kumar, S. Kumar, S.K. Tyagi, Design, development and technological advancement in the biomass cookstoves: a review, *Renew. Sustain. Energy Rev.* 26 \(2013\) 265–285.](#)
- [3] D. Lyle, *The Book of Masonry Stoves: Rediscovering an Old Way of Warming*, Chelsea Green Publishing Company, 1984.
- [4] M. Bryden, D. Still, P. Scott, G. Hoffa, D. Ogle, R. Bailis, et al., *Design Principles for Wood Burning Cook Stoves*, report no. EPA-402-K-05-004. US Environmental Protection Agency, Office of Air and Radiation, 2005.
- [5] M. Bryden, D. Still, D. Ogle, N. MacCarty, *Designing Improved Wood Burning Heating Stoves*, Aprovecho Research Center, 2005.
- [6] I. Evans, L. Jackson, *Rocket Mass Heaters: Superefficient Woodstoves YOU Can Build*, third ed., Cob Cottage Company, 2014.
- [7] <<http://www.ernieandERICA.info/>>, (accessed 13.07.15).
- [8] <<http://www.permies.com/>>, (accessed 13.07.15).
- [9] [D. Menghini, F.S. Marra, C. Allouis, F. Beretta, Effect of excess air on the optimization of heating appliances for biomass combustion, *Exp. Therm. Fluid Sci.* 32 \(2008\) 1371–1380.](#)
- [10] [E. Felaco, I. Gasser, Modelling, asymptotic analysis and simulation of the gas dynamics in a chimney, *J. Math. Ind.* 3 \(2013\) 3.](#)
- [11] [J. Saastamoinen, P. Tuomaala, T. Paloposki, K. Klobut, Simplified dynamic model for heat input and output of heat storing stoves, *Appl. Therm. Eng.* 25 \(2005\) 2878–2890.](#)
- [12] [N.A. MacCarty, K.M. Bryden, Modeling of household biomass cookstoves: a review, *Energy Sustain. Dev.* 26 \(2015\) 1–13.](#)
- [13] N.A. MacCarty, A zonal model to aid in the design of household biomass cookstoves, (2013). Iowa State University. Graduate Theses and Dissertations. Paper 13589.
- [14] [N. MacCarty, K.M. Bryden, A heat transfer model for the conceptual design of a biomass cookstove for developing countries, *Proceedings of the ASME 2013 International Design Engineering Technical Conference & Computers and Information in Engineering Conference IDETC/CIE 2013, August 4–7, 2013, Portland, Oregon. DETC2013-12650.*](#)
- [15] [J. Agenbroad, M. DeFoort, A. Kirkpatrick, C. Kreutzer, A simplified model for understanding natural convection driven biomass cooking stoves – part 1: setup and baseline validation, *Energy Sustain. Dev.* 15 \(2011\) 160–168.](#)
- [16] P.J. Pritchard, Fox and McDonald's *Introduction to Fluid Mechanics*, eighth ed., John Wiley & Sons, 2011.
- [17] [T.L. Bergman, A.S. Lavine, F.P. Incropera, D.D. DeWitt, *Introduction to Heat Transfer*, sixth ed., John Wiley & Sons, 2011.](#)
- [18] [B.R. Munson, T.H. Okiishi, W.W. Huebsch, A.P. Rothmayer, *Fundamental of Fluid Mechanics*, seventh ed., John Wiley & Sons, 2013.](#)
- [19] R.H. Howell, W.J. Coad, H.J. Sauer, *Principles of Heating Ventilating and Air Conditioning*, seventh ed., ASHRAE, 2013.
- [20] [M.J. Spearpoint, J.G. Quintiere, Predicting the burning of wood using an integral model, *Combust. Flame* 123 \(3\) \(2000\) 308–325.](#)